Langmuir

Article

pubs.acs.org/Langmuir

Self-Assembly of Amphiphilic Glycoconjugates into Lectin-Adhesive Nanoparticles

Alexandre G. Dal Bó,[†,‡] Valdir Soldi,[‡] Fernando C. Giacomelli,[§] Christophe Travelet,[†] Bruno Jean,[†] Isabelle Pignot-Paintrand,[†] Redouane Borsali,[†] and Sébastien Fort*[,†]

[†]Centre de Recherches sur les Macromolécules Végétales (CERMAV-CNRS), BP 53, F-38041 Grenoble Cedex 9, France (affiliated with Université Joseph Fourier Grenoble 1 and a member of the Institut de Chimie Moléculaire de Grenoble)

[‡]Departamento de Química, Universidade Federal de Santa Catarina, 88040-900 Florianópolis − SC, Brazil

[§]Centro de Ciências Naturais e Humanas, Universidade Federal do ABC, 09210-170 Santo André − SP, Brazil

Supporting Information

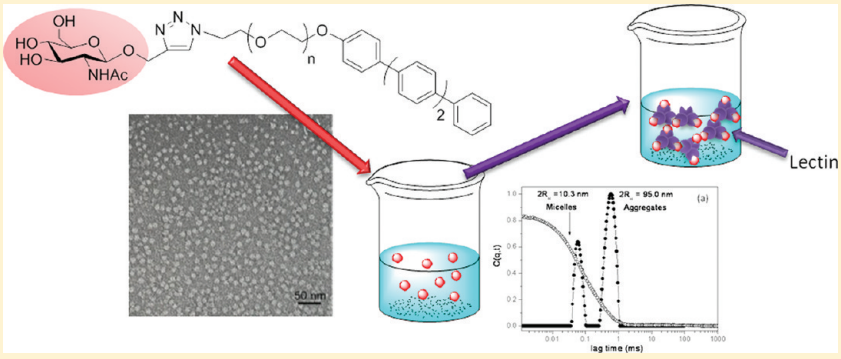

ABSTRACT: This work describes the synthesis and self-assembly of carbohydrate-clicked rod−coil amphiphilic systems. Copper-catalyzed Huisgen cycloaddition was efficiently employed to functionalize the hydrophilic extremity of PEG-*b*-tetra(*p*-phenylene) conjugates by lactose and *N*-acetyl-glucosamine ligands. The resulting amphiphilic systems spontaneously self-assembled into nanoparticles when dissolved in aqueous media, as evidenced by dynamic light scattering (DLS), transmission electron microscopy (TEM), and small-angle X-ray scattering (SAXS). The formation of highly monodisperse micelles having a mean diameter of 10 nm was observed for systems containing a PEG 900 core, and a decrease in the hydrophilic moiety (PEG 600) led to the formation of vesicles with a broader size distribution. The presence of carbohydrate residues on the surfaces of the micelles and their ability to establish specific interactions with wheat germ agglutinin (WGA) and peanut agglutinin (PNA) were further highlighted by light-scattering measurements, thus confirming the attractive applications of such sugar micelles in biosensor devices.

INTRODUCTION

The design of functional nanoparticles possessing optical, magnetic, or bioaffinity properties is currently the subject of intensive research with important outcomes in medicine for cancer diagnosis and therapy.[1,2] Although it is well established that nanoparticles preferentially localize at the tumors as a result of the enhanced permeation and retention effect,[3,4] much effort is now being devoted to the preparation of functionalized delivery systems, allowing active targeting while sparing healthy cells.[5] The selective accumulation of drugs or molecular probes for imaging in the tumor tissues can be achieved through receptor−ligand interactions with carbohydrate-decorated nanoparticles.[6] Indeed, interactions taking place at the cell surface between oligosaccharides and carbohydrate binding proteins known as lectins play a crucial role in standard and pathological processes including fertilization, viral and bacterial infections, the inflammatory response, cell adhesion, and metastatic spreading.[7] It has been shown that lectins affect tumor cell survival, adhesion to the endothelium, and the extracellular matrix as well as tumor vascularization and other processes that are crucial to metastatic spread and growth.[8,9] The development of nanoparticles whose corona is decorated by carbohydrates aimed at targeting certain lectins and inversely the development of those whose corona is covered by lectins that bind to cell-surface carbohydrates are considered to be promising ways to detect cancer at an early stage and to improve drug delivery.[10−13]

A practical and efficient way to prepare well-defined nanoparticles, among others, relies on the self-assembly of amphiphilic molecules. In aqueous solution, the spontaneous self-organization of amphiphiles driven by noncovalent interactions including hydrophobic, electrostatic, $\pi-\pi$ stacking,

Received: November 8, 2011
Revised: December 14, 2011
Published: December 15, 2011

and hydrogen bonding can induce well-defined nanostructures.[14] These organized nanostructures can be rationalized in terms of the hydrophobic volume fraction, molar mass, and flexibility of the amphiphile, providing access to a wide range of morphologies including spherical and cylindrical micelles, vesicles, nanofibers, toroids, tubes, and so forth.[15−18] The preparation of particles from amphiphilic graft or block copolymers containing a polysaccharidic part including dextran, chitosan, hyaluronic acid, or water-soluble cellulose derivatives is abundantly documented.[19,20] Although biomass-derived polysaccharides provide a valuable scaffold for the elaboration of nanoparticles, they barely interact with lectins. The binding of lectins typically involves only the two or three terminal sugar residues of the mammalian glycans including galactose, mannose, *N*-acetyl neuraminic acid, fucose, or *N*-acetyl-glucosamine.[21] Recently, Kim et al. reported a series of carbohydrate amphiphilic systems prepared from PEG scaffolds and polyaromatic hydrophobic blocks.[22,23] Self-assembled nano-objects of different sizes and morphologies were obtained in water depending on the molecular architecture and the volume fraction of each constituent, and the bioavailability of the sugar units for *E. coli* receptors was confirmed.

With the aim of developing a practical and versatile way to prepare self-assembled nanoparticles whose surfaces are functionalized by carbohydrates, we have designed azido-terminated rod−coil amphiphiles consisting of a rigid tetra(*p*-phenylene) and a flexible oligo(ethylene oxide) segment. On one hand, PEGylation offers a unique approach to improving the solubility of hydrophobic molecules in aqueous media, and it is well known to reduce clearance rates of drug-delivery systems and proteins in vivo.[24−26] On the other hand, oligophenylenes are linear hydrophobic stiff molecules with promising applications in biosensing devices due to their photoluminescent and electroluminescent properties[27] as well as their conducting properties when doped with oxidizing or reducing reagents.[28] Although their processability is generally hampered by solubility issues, derivatization with oligoethylene groups improves their manipulation and can lead to self-assembled nanostructures. Block copolymers exhibiting strong fluorescence in the blue region and consisting of alternating tetra(*p*-phenylene) and solubilizing poly(ethylene glycol) spacers were reported by Hargadon et al. using a Suzuki coupling strategy.[29] Oligophenylene-based conjugates were also shown to adopt a wide range of self-assembled nanostructures including ribbons, nanotubes, and micelles.[30−34]

In the present work, we report the synthesis, self-assembly, and interaction study of new amphiphilic systems targeting lectins prepared using the click-chemistry grafting of propargylated carbohydrates onto azido-PEG-tetra(*p*-phenylene). Poly(ethylene glycol) having an average molar mass of 900 was selected to act as a flexible hydrophilic spacer of the appropriate size to provide amphiphiles with a hydrophobic volume fraction of close to 20% that is required for the formation of spherical micelles.[14] An amphiphile incorporating a shorter PEG segment (MW 600) was also prepared in order to evaluate the influence of the hydrophilic/lipophilic balance on the resulting self-assembled particles. Propargyl β-lactoside and *N*-acetyl-β-D-glucosaminide were conjugated by popular, efficient copper-catalyzed Huisgen cycloaddition[35,36] to the azide-terminated-PEG-tetra(*p*-phenylene). The self-assembled nanoparticles and their lectin adhesion properties were characterized by light scattering and microscopy techniques.

EXPERIMENTAL SECTION

Materials. All reagents were of commercial grade, and they were used as received unless otherwise noted. *Triticum vulgaris* (wheat germ) lectin (WGA) and *Arachis hypogaea* (peanut) lectin (PNA) were obtained from EY Laboratories, Inc. The solvents were dried and distilled according to literature procedures before use. The reactions were monitored by TLC using silica gel 60 F254 precoated plates (E. Merck, Darmstadt, Germany), and detection was achieved by exposure to iodine vapors or by charring with 3:45:45 H_2SO_4/MeOH/H_2O. For flash chromatography, E. Merck silica gel 60 was used.

Characterization of the Amphiphilic Systems. NMR spectra were recorded on a Bruker AC 300 or Bruker Avance 400 spectrometer at 25 °C, and they were calibrated against the residual signal of the solvent. Mass spectra were recorded on a Bruker Daltonics Autoflex apparatus for MALDI and on a Waters Micromass ZQ spectrometer for ESI experiments. Infrared (IR) spectra were recorded using a Perkin-Elmer Spectrum RXI FTIR spectrometer.

Synthesis. Propargyl 2-acetamido-2-deoxy-β-D-glucopyranoside[37] and propargyl β-lactoside[38] were prepared as previously reported in the literature. Synthesis and characterization data for compounds **1**−**7** are described in the Supporting Information.

Nanoparticle Preparation. The suspensions of nanoparticles (aqueous micellar solutions, C_p = 0.2−1.0 mg/mL) were prepared by direct dissolution of the amphiphilic systems in Milli-Q water or in phosphate-buffered saline solution (PBS, 10 mM, pH 7.2, 1 mM $CaCl_2$, 1 mM $MnCl_2$) and stirred for 24 h at 25 °C. The solutions were then filtered using 0.45-μm-pore-size nylon membrane filters in order to remove dust and large aggregates.

Characterization of the Nanoparticles. *Dynamic Light Scattering (DLS).* The size and polydispersity of the nanoparticles were accessed using DLS measurements. The experiments were performed using an ALV/CG6-8F goniometer equipped with a 35 mW red helium−neon linearly polarized laser (λ = 632.8 nm) and an ALV/LSE-5004 multiple tau digital correlator with a 125 ns initial sampling time.[39] The samples were kept at 25 °C. The accessible scattering angle of the equipment ranges from 12 to 155°. All samples were systematically studied at 90°, and some of them were studied at different scattering angles varying from 40 to 140°. The solutions were loaded into 10-mm-diameter glass cells. The minimum sample volume required for an experiment was 0.8 mL. The data were acquired with the ALV correlator control software, and the counting time for each sample was typically 300 s. The distributions of relaxation times, $A(t)$, were obtained using the CONTIN analysis applied to the autocorrelation functions, $C(q, t)$.[40] The relaxation times, which are denoted as τ, correspond to the local maxima of the distributions $A(t)$, and the relaxation frequencies (Γ) are equal to $^1/_\tau$.[41] The diffusion coefficient (D) of the nanoparticles at a given copolymer concentration (C_p) is calculated from eq 1

$$\left.\frac{\Gamma}{q^2}\right|_{q\to 0} = D \tag{1}$$

where q is the modulus of the scattering vector that is defined as

$$q = \frac{4\pi n}{\lambda}\sin\left(\frac{\theta}{2}\right) \tag{2}$$

with λ being the wavelength of the incident laser beam, n being the refractive index of the pure solvent (1.33 for water), and θ being the scattering angle. The hydrodynamic radius (R_H) (or diameter, $2R_H$) was calculated from the Stokes−Einstein equation given in eq 3

$$R_H = \left.\frac{k_B T q^2}{6\pi\eta\Gamma}\right|_{q\to 0} = \frac{k_B T}{6\pi\eta D} \tag{3}$$

where k_B is the Boltzmann constant, T is the temperature of the sample, and η is the viscosity of the pure solvent (water in this case).[42] The radius of gyration (R_G) was calculated from the elastic part ($I(q)$) of the scattering intensity using the Guinier approximation as follows

dx.doi.org/10.1021/la204388h | *Langmuir* 2012, 28, 1418−1426

Scheme 1. Synthesis Strategy Used in the Preparation of $\phi_4PEG_{900}GlcNAc$ (6a), $\phi_4PEG_{600}GlcNAc$ (6b), and $\phi_4PEG_{900}Lac$ (7)[a]

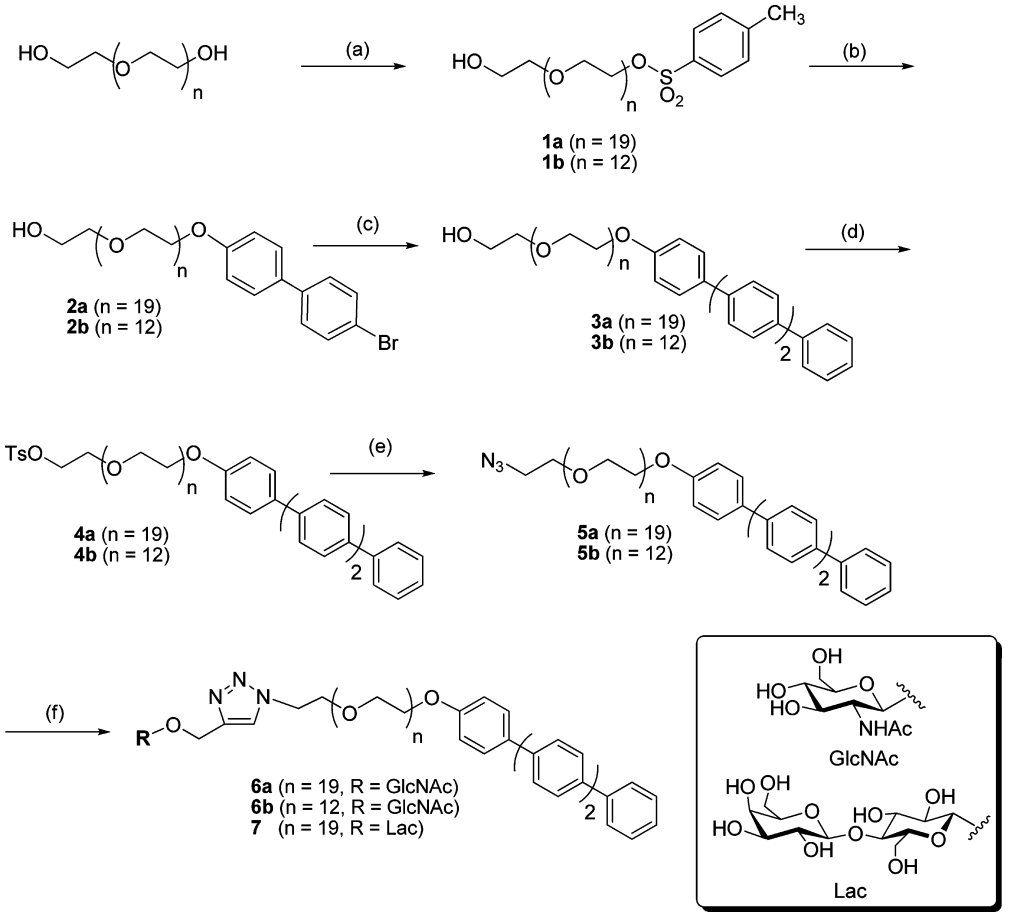

[a](a) TsCl, Ag_2O, KI, CH_2Cl_2 (**1a**, 55%; **1b**, 58%). (b) 4-(4-Bromophenyl)phenol, K_2CO_3, CH_3CN (**2a**, 52%; **2b**, 52%). (c) 4-Biphenyl boronic acid, $(PPh_3)_4Pd$, Na_2CO_3, THF (**3a**, 50%; **3b**, 50%). (d) TsCl, $C_6H_{15}N$, CH_2Cl_2 (**4a**, 87%; **4b**, 75%). (e) NaN_3, DMF (**5a**, 85%; **5b**, 80%). (f) $CuSO_4$, sodium ascorbate, propargyl 2-*N*-acetamido-2-deoxy-β-D-glucopyranoside or propargyl β-lactoside, H_2O/THF (**6a**, 60%; **6b**, 53%; **7**, 55%).

$$\ln I = \ln I_0 - \frac{1}{3}q^2 R_G{}^2 \quad (4)$$

where I is the scattering intensity and I_0 is the scattering intensity at $q = 0$.

Transmission Electron Microscopy (TEM). Sample preparation was done as follows: 4 μL of an aqueous micellar solution was dropped onto a glow-discharged carbon-coated copper grid. Then 4 μL of a 2% w/v uranyl acetate negative stain was added prior to complete drying. After a few minutes, the excess liquid was blotted with a filter paper and the grid was allowed to dry. The specimens were observed using a Philips CM200 microscope operated at 80 kV. Images were recorded on Kodak SO163 films, and the negatives were digitized off-line using a Kodak Mega plus CCD camera. The mean diameter of the nanoparticles (n = 50) was determined with Scandium software.

Small-Angle X-ray Scattering (SAXS). The systems were investigated by SAXS at French CRG beamline D2AM-BM02 of the European Synchrotron Radiation Facility (ESRF) and at the Brazilian Synchrotron Light Laboratory (LNLS). The results reported herein were obtained at the ESRF. The wavelength (λ) of the incoming beam and the sample-to-detector distance were chosen in such a way that the q range could be covered from 0.15 to 3.0 nm^{-1}. The samples were loaded into sealed borosilicate capillaries (~2 mm diameter). The collimated beam crossed the samples and was scattered to an indirect-illumination CCD detector (Princeton Instruments). In all cases, the 2D images were found to be isotropic, and they were corrected by taking into account the detector dark noise and normalized by the sample transmission. The $I(q)$ versus q curves resulting from the 360° azimuthal integration of the 2D patterns were further corrected by the subtraction of the scattering of the pure solvent (water) and were fitted by using the spherical copolymer micelle model developed by Pedersen and Gerstenberg.[43] The fitting procedures and other analyses were performed using the SASfit software, which makes use of the least-squares fitting approach for minimizing the χ^2 parameter. The SASfit software package was developed by Kohlbrecher and is available online.[44]

RESULTS AND DISCUSSION

Synthesis of the Amphiphiles. The synthesis of glycosylated rod−coil amphiphiles consisting of tetra(*p*-phenylene) and poly(ethylene oxide) segments is depicted in Scheme 1. The selective monotosylation of PEG (MW 900 and 600) was carried out in the presence of silver oxide (Ag_2O) and a catalytic amount of potassium iodide (KI) as reported by Bouzide et al.[45] The tetra-(*p*-phenylene) hydrophobic block was then installed in a two-step sequence consisting of the nucleophilic substitution of the tosyl group by 4′-bromo-(1,1′-biphenyl)-4-ol followed by palladium-catalyzed Suzuki coupling with 4′-biphenyl boronic acid as described earlier by Kim et al.[23] Azidation of the second extremity of the PEG block was further carried out through a tosylated intermediate affording clickable amphiphiles $\phi_4PEG_{900}N_3$ (**5a**) and $\phi_4PEG_{600}N_3$ (**5b**). The absorption peak of the N_3 group at 2100 cm^{-1} observed by infrared spectroscopy and the ^{13}C signal of the methylene carbon adjacent to the azide group at 50.7 ppm seen by NMR

dx.doi.org/10.1021/la204388h | *Langmuir* 2012, 28, 1418−1426

confirmed the efficiency of this transformation. Propargyl β-glycosides of *N*-acetyl-glucosamine and lactose were introduced at the polar head of the amphiphile by copper-catalyzed Huisgen cycloaddition. The reaction was carried out at 40 °C with the copper/ascorbate catalytic system in a water/THF mixture to ensure good solubility of the reactants. Glycosylated conjugates $\phi_4PEG_{900}GlcNAc$ (**6a**), $\phi_4PEG_{600}GlcNAc$ (**6b**), and $\phi_4PEG_{900}Lac$ (**7**) were respectively isolated in 60, 53, and 55% yields after purification by silica gel chromatography. The IR spectra confirmed the coupling efficiency assessed by the disappearance of the signal due to the azide group. Finally, the structures of the three glycosylated amphiphiles were unambiguously confirmed by NMR spectroscopy in DMSO-d_6, a good solvent for each part of the molecule, and by MALDI-TOF-MS.

Both ^1H and ^{13}C NMR spectra displayed characteristic signals of the aromatic groups, the ethylenoxide part and the carbohydrate units, and signals of the triazolyl ring. Figure 1 depicts as a representative example the ^{13}C NMR spectra of **6a** in DMSO-d_6.

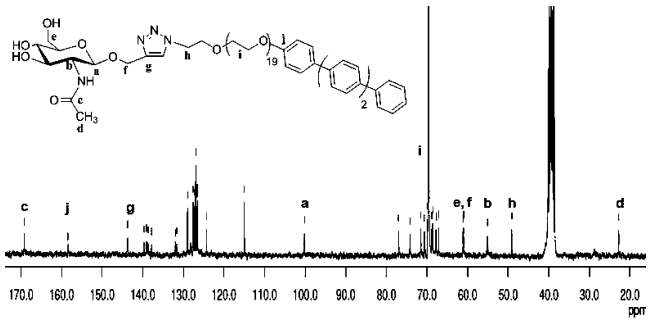

Figure 1. ^{13}C spectra of $\phi_4PEG_{900}GlcNAc$ (**6a**) in DMSO-d_6.

Self-Assembly of the PEG_{900}-Based Amphiphiles. The above synthesized PEG_{900}-based amphiphiles were self-assembled as described in the Experimental Section, and the resulting auto-organizations were probed with DLS. One can observe two well-defined peaks in the relaxation−time distribution of **5a** (Figure 2a) highlighting two distributions of particles whose average sizes are $2R_H$ = 10.3 and 95.0 nm. They can be reasonably attributed to micelles for the small-scale structures and to ill-defined aggregates for the large-scale structures. Indeed, the predicted fully extended length for **5a** is 10.2 nm, which is compatible with the experimental value ($2R_H$ = 10.3 nm). At that point, it should be kept in mind that the distribution presented in Figure 2 is, by definition, a mass-weighted distribution. Consequently, although the peak corresponding to the large-scale structures is the most intense, the number of aggregates is very small. Indeed, from a more quantitative point of view, using the hypothesis that hard-sphere-like particles are present and that the small- and large-scale structures have the same density, the aggregates represent only 0.2% of the total number of particles.[46]

The minor percentage of aggregates in the system was confirmed in the TEM image (Figure 2b) where one can clearly observe spherical micelles whose average diameter is 9.9 ± 1.9 nm, which is consistent with the particle size of the main distribution in number observed by DLS. Such results are very similar to those obtained by Lee et al. when investigating similar systems.[22]

The glycosylation of **5a** with a GlcNAc or a lactose group did not significantly change its hydrophilic/hydrophobic balance, and amphiphiles **6a** and **7** self-assembled into nanoparticles of similar size when dissolved in water as evidenced by DLS and TEM. The insets in Figure 3a,b depict the typical angular variations (plotted as a function of q^2) of the relaxation frequency $\Gamma = {}^1/_\tau$. They are clearly attributed to Brownian diffusive motions of particles. The hydrodynamic radii of **6a** and **7** were calculated from the relaxation frequencies using the Stokes−Einstein equation (eq 3). Regarding the micelles, the values are practically the same as the value obtained before the click chemistry reaction (amphiphile **5a**): $2R_H$ = 10 nm. TEM images (Figure 3c,d) confirmed the formation of mainly nanosized spherical structures having mean diameters of 12.9 ± 1.9 and 10.9 ± 1.9 nm for GlcNAc and the lactose amphiphile, respectively. Although the dynamic light scattering technique is extremely sensitive to the presence of large aggregates, their real number in the current system is again negligible as mentioned hereabove.

The morphology, size, and structure of nanoparticles are mainly dependent on the balance of the forces of attraction and repulsion between the different blocks of the amphiphiles. The spherical micelles found here are in agreement with the volume fraction in the hydrophobic region, $\varphi < {}^1/_3$.[14,16,47] Indeed, the calculated hydrophobic volume fractions of **5a**, **6a**, and **7** based on the density of each constituent were equal to 0.29, 0.24, and

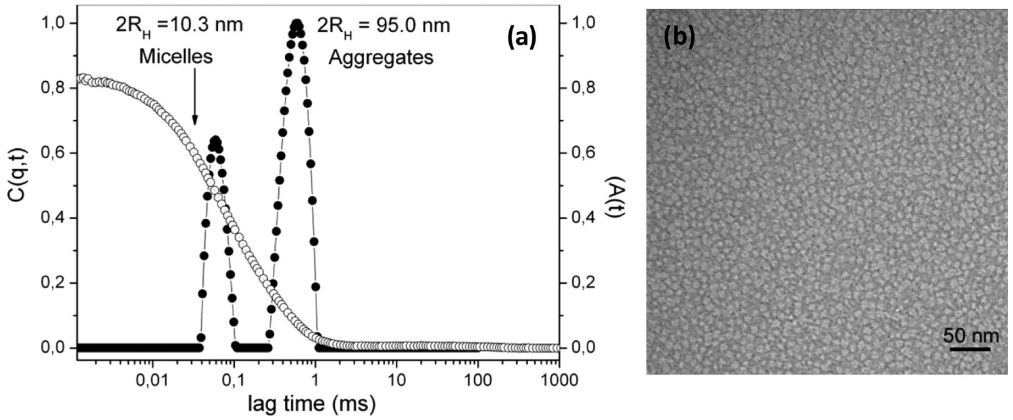

Figure 2. (a) Dynamic light scattering autocorrelation function (○) and relaxation-time distribution (●) of $\phi_4PEG_{900}N_3$ **5a** in water (conditions: [**5a**] = 0.5 mg/mL, scattering angle θ = 90°, and temperature = 25 °C). (b) TEM image of self-assembled $\phi_4PEG_{900}N_3$ **5a** nanoparticles in water.

dx.doi.org/10.1021/la204388h | *Langmuir* 2012, 28, 1418−1426

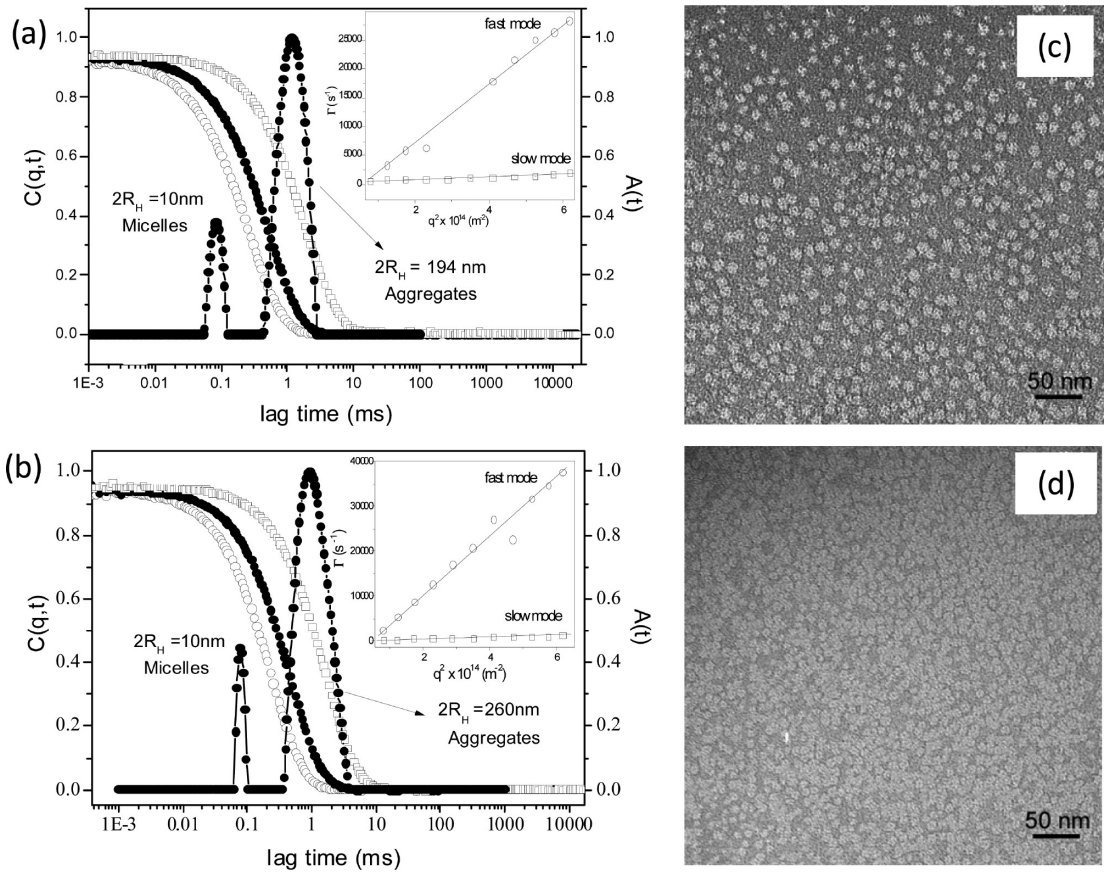

Figure 3. (a, b) Dynamic light scattering autocorrelation function measured at scattering angles of 50 (□), 90 (●), and 130° (○) and the relaxation−time distributions (−) of ϕ_4PEG$_{900}$GlcNAc **6a** and ϕ_4PEG$_{900}$Lac **7** in water (conditions: [**6a**/**7**] = 0.5 mg/mL; temperature = 25 °C). The insets show the dependences of the relaxation frequency (Γ) on the square of the modulus of the wave vector (q^2). (c, d) TEM observation of spherical nanoparticles formed in water from ϕ_4PEG$_{900}$GlcNAc **6a** and ϕ_4PEG$_{900}$Lac **7**. The structures were seen after negative staining.

0.23, respectively. Therefore, spherical micelles are expected.[14,16,42]

In addition to DLS and TEM experiments, SAXS measurements were performed in order to probe the size, shape, and internal structure of the scattering particles. The scattering intensity $I(q)$ of an isotropic solution of highly regular particles embedded in a matrix with a constant electron density, after normalization with the background scattering of the solvent, is given by

$$I(q) = N_p\, P(q)\, S(q) \qquad (5)$$

where N_p is the number of scattering particles per unit volume, $P(q)$ is the form factor of an individual particle, and $S(q)$ is the structure factor arising from long-range correlations between scattering centers. For widely separated systems, as in the case of solutions with low copolymer contents, $S(q) \approx 1$; consequently, $I(q)$ represents the form factor $P(q)$ that reflects the size and shape of the scattering objects.

Figure 4 shows the SAXS patterns of **6a** (top) and **7** (bottom) in water at 25 °C and at C_P = 40 mg/mL. Such a copolymer concentration gives reasonable signal-to-noise statistics without affecting the micellar structure, still with no interference from $S(q)$. Furthermore, the presence of a small number of ill-defined aggregates is suggested by the X-ray scattering intensity upturn in the low-q region, as evidenced by the DLS experiments.

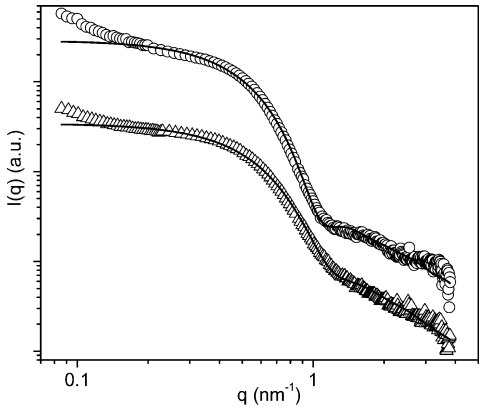

Figure 4. Experimental SAXS data (symbols) and respective curve fittings using the spherical copolymer micelle model (lines) for solutions containing **6a** (top) and **7** (bottom) dissolved in water at C_P = 40 mg/mL and 25 °C.

The high-q-range profile for the self-assembled nanoparticles is dominated by the coil nature of the chain at the surface. This is due to the fact that the scattering contribution coming from the PEG chains dissolved in the micellar corona dominates the X-ray scattering profile in the high-q region, which is ideally dictated by the Debye function and therefore by a nearly q^{-2} dependence depending on the conformation of the flexible polymer chains. Indeed, the SAXS profiles could be satisfactorily fitted by using the so-called spherical copolymer

dx.doi.org/10.1021/la204388h | *Langmuir* 2012, 28, 1418−1426

micelle model formerly developed by Pedersen and Gerstenberg.[43] Such a model describes the scattering of micelles consisting of a homogeneous spherical core having corona chains that follow Gaussian statistics attached to the surface of the core as shown by the cartoon in Figure 5. The micellar form

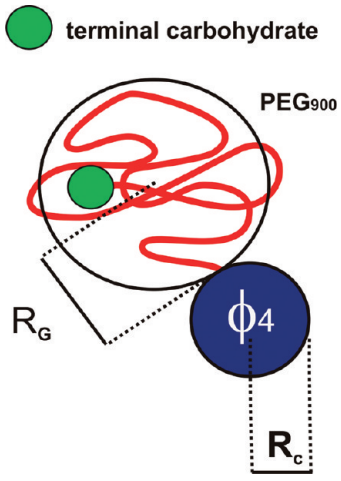

Figure 5. Schematic representation for the micellar form factor analysis according to the spherical copolymer micelle model. It considers a dense spherical core of radius R_c and Gaussian chains with radius of gyration $R_{G(chain)}$ attached to the core.

factor $P_{mic}(q)$ involves four contributions that are detailed in ref 43.

This model has a large number of fitting parameters, namely, $R_{G(chain)}$, d, R_c, N_{agg}, and the excess scattering-length density of the core and corona forming blocks (β_{core} and β_{chain}). Therefore, it is usually not possible to get a single set of fitting parameters if some of the parameters are not preset, and generally the fittings provide ambiguous results. Hence, during the fitting procedures parameters β_{chain} (7.30×10^{-12} cm) and d (explained in detail in ref 43) were kept fixed. The model does not prevent the chains from penetrating into the core region, but this can be artificially avoided by displacing the starting point of the Gaussian chains. Indeed, by setting $d = 1$, the PEG chains are displaced to a value of $R \approx R_C + R_G$ away from the center of the particle. The value of β_{chain} was calculated in the following way

$$\beta_{chain} = NV_{PEG}(\sigma_{PEG} - \sigma_{solvent}) \quad (6)$$

where N is the degree of polymerization of the polymer segment, V_{PEG} is the volume of one PEG monomer unit, σ_{PEG} is the scattering-length density of the polymer segment, and σ_{solv} is the scattering-length density of the solvent. The volume occupied by a single monomer unit V_{PEG} was determined by taking into account the homopolymer density (d_{PEG} = 1.08 g/mL), and the values of the scattering-length densities of the solvent ($\sigma_{water} = 9.42 \times 10^{10}$ cm^{-2}) and monomer unit ($\sigma_{PEG} = 9.99 \times 10^{10}$ cm^{-2}) were calculated using the average chemical composition of each component and its mass density (d_x)

$$\sigma_x = \frac{b_e d_x N_A}{M_x} \sum_i n_i z_i \quad (7)$$

where x accounts for H_2O or PEG, N_A is Avogadro's number, and $n_i z_i$ is the number of electrons in each unit. Finally, b_e is the Thomson scattering length (the scattering length of an electron, $b_e = 2.817 \times 10^{-13}$ cm).

The fitting parameters were therefore N_{agg}, R_c, $R_{G(chain)}$, and β_{core}. In Figure 4, the solid lines correspond to the best fits achieved using the spherical copolymer micelle model. The high quality of the fits can be straightforwardly noticed, indeed attesting to the spherical topology of the hydrophobic micellar core and the Gaussian conformation of the PEG chains in the corona. The parameters extracted from the SAXS curve fittings are listed in Table 1.

The determined values of β_{core} confirm that the micellar-like aggregates herein investigated consist of weakly scattering cores ($\beta_{core} < \beta_{chain}$). The low value of β_{core} thus suggests a swelling of the micellar core by the solvent. Such a swelling is geometrically possible considering the conformation of the tetra(*p*-phenylene) block. The core radius (R_c) was found to be ~1.9−2.5 nm, which is compatible with a micellar core composed of tetra(*p*-phenylene) blocks whose length is 1.8 nm and with the R_G of the PEG corona chains of ~0.9−1.2 nm. The reduction in the core radius is balanced by the slight increase in $R_{G(chain)}$, and the micellar dimension (R_{mic}) calculated to be $R_c + 2R_G$ was found to be in the range of 4.1−4.3 nm. One should keep in mind that for spherically shaped (micellar core−shell) objects the structure-sensitive parameter ρ ($\rho = R_G/R_H$) is theoretically equal to 0.774.[48] Therefore, the whole micellar size (R_{mic}) monitored by SAXS should be smaller than R_H as monitored by DLS ($R_H \approx 5$ nm). The similar R_{mic} values reported for bare particles and for those decorated with carbohydrates suggest a negligible influence of the sugar units in the self-assembly. The size and morphology of the particles are mainly dictated by the oligophenylene and PEG blocks. This result is consistent with previous findings on the self-assembly of glycosylated PEG-stearate amphiphiles.[49] As expected, the aggregation numbers N_{agg} were related to the steric hindrance of the polar end-chain of the amphiphiles, and these values dropped from 59 to 41 and 30 from the azido to the monosaccharide and disaccharide derivatives, respectively.

Because R_c and N_{agg} had been determined, the core surface area available per PEG chain in the micellar corona (A_c) could be calculated with eq 8:

Table 1. Structural Parameters of the Scattering Nano-objects Determined from the Fits of the SAXS Spectra Using the Spherical Copolymer Micelle Model[a]

copolymer	R_c (nm)	R_G (nm)	L(nm)	R_{mic} (nm)	N	β_{core} (10^{-12} cm)	A_c (nm^2)	a
ϕ_4PEG$_{900}$N$_3$	1.9	1.2	2.4	4.3	59	2.6	0.8	1.7
ϕ_4PEG$_{900}$GlcNAc	2.5	0.9	1.8	4.3	41	2.6	1.9	1.7
ϕ_4PEG$_{900}$Lac	2.1	1.0	2.0	4.1	30	2.6	1.8	2.0

[a] R_c, core radius; R_G, radius of gyration; $L = 2R_G$, thickness of the micellar corona; $R_{mic} = R_c + L$, micellar dimension; N_{agg}, aggregation number; β_{core}, excess scattering-length density of the core-forming blocks; A_c, core surface area available per PEG chain in the micellar corona; and a, exponent of the q dependence. $L = 2R_G$ (thickness of the micellar corona). $R_{mic} = R_c + L$

dx.doi.org/10.1021/la204388h | *Langmuir* 2012, 28, 1418−1426

$$A_c = \frac{4\pi R_c^{\,2}}{N_{agg}} \quad (8)$$

These values are also listed in Table 1. The conformation of the PEG chains should depend on such physical chemical variables: as A_c decreases, a larger R_G might be expected, and thus the smaller the area available on the core surface, the more stretched the configuration of PEG chains that is assumed. In such cases, the q^{-a} slope in the high-q range reveals important information about the chain statistics,[50] namely, $a = 2$ for Gaussian chains (polymers in a θ solvent), $a \approx 1.67$ for chains with excluded volume (polymer in a good solvent), and $a = 1$ for rigid rodlike chains. The values of a (Table 1) suggest that the PEG chains in the ϕ_4PEG$_{900}$GlcNAc micelles are slightly more stretched compared to those in ϕ_4PEG$_{900}$Lac.

Self-Assembly of the PEG$_{600}$-Based Amphiphiles. In addition to the PEG$_{900}$ glycoconjugates, PEG$_{600}$-based derivatives were synthesized and their self-assembly was investigated (Figure 6). One could expect to produce particles of different sizes and morphologies by changing the hydrophilic/hydrophobic balance of the amphiphiles. In the current case, the hydrophobic polyaromatic segment remained constant and the PEG hydrophilic region was reduced to PEG$_{600}$.

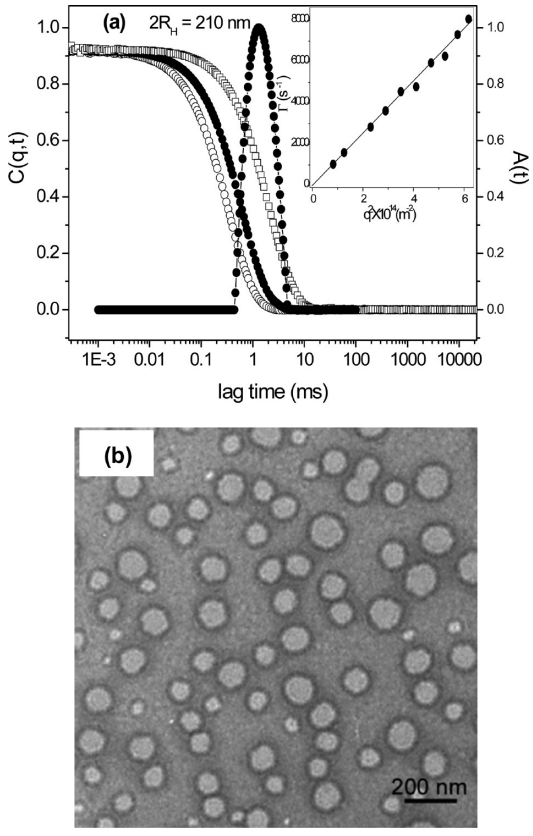

Figure 6. (a) Dynamic light scattering autocorrelation function measured at scattering angles of 50 (□), 90 (●), and 130° (○) and relaxation−time distribution (−) of **5b** in water (conditions: [**5b**] = 0.4 mg/mL; temperature = 25 °C). The inset shows the variation of the relaxation frequency (Γ) as a function of the square of the modulus of the wave vector (q^2). (b) TEM observation morphology resulting from the self-assembly of the **5b** amphiphile in water. The observation was made after negative staining.

As expected, the reduction of the PEG size had a dramatic influence on the size and morphology of the nano-objects resulting from the self-assembly of **5b**. The inset in Figure 6a depicts a linear dependence of the relaxation frequency versus q^2 showing that Brownian diffusive motions of particles are observed. However, contrary to the longer PEG$_{900}$-based amphiphiles, the PEG$_{600}$-based amphiphiles form nanoparticles in water whose size distribution is polydisperse and centered on $2R_H \approx 210$ nm. These findings were confirmed by TEM observations (Figure 6b) where one could reasonably see the presence of nanoparticles with a vesicular morphology. Particles of similar size were also observed with **6b** (Supporting Information), confirming a negligible influence of the carbohydrate group in the self-assembly.

Consequently, reducing the hydrophilic volume fraction of the studied amphiphilic systems led to completely different self-assemblies in term of size and multimodality. Furthermore, in order to have a more precise idea of the morphology of the present species, the system was also investigated using static light scattering (SLS) measurements by varying the scattering angle (θ) from 30 to 150° with a 15° stepwise increase. The Guinier plot profile of **5b** shows basically a straight line and no upturn at small q values, indicating that large aggregates are not present and that the contribution of the light-scattering intensity comes from a monomodal size distribution of particles (Supporting Information). The R_G value, determined from the slope, was equal to 103 nm, leading to an experimental ratio of $R_G/R_H = 0.98$ that is in reasonable agreement with the theoretical value ($R_G/R_H \approx 1.0$) for vesicular morphologies.[51] Thus, light-scattering data together with TEM images suggest that the PEG$_{600}$ amphiphiles self-assemble into vesicular morphologies, as one would expect from their hydrophobic volume fractions (0.38 and 0.31 for **5b** and **6b**, respectively).[14,16,42]

Specific Interaction of the Nanoparticles with WGA and PNA Lectins. The investigation of lectin binding was further carried out by DLS to demonstrate the bioavailability of the sugar residues on the surfaces of the micellar nanoparticles. Wheat germ agglutinin (WGA) and peanut (*Arachis hypogaea*) lectin (PNA) are lectins showing specificities for β-*N*-acetylglucosamine and galactose, respectively.[52,53] Each self-assembled glycosidic system was first incubated with a nonbinding lectin to evaluate its possible nonspecific interaction. No modification of the autocorrelation curves was observed after the addition of WGA to the lactose system or after the addition of PNA to the GlcNAc-decorated particles, thus confirming both the specificity of the proteins and the absence of nonspecific binding (Supporting Information). However, as shown in Figure 7a, the interaction of lactosyl-covered spherical micelles with PNA lectin significantly increases the micellar hydrodynamic radius R_H by almost 50% (from 11.8 to 17.2 nm). It clearly shows the specific interaction of the protein with lactose groups that are definitely available on the shell of the nanoparticles.

Modifications in the distributions of relaxation times (i.e., shifts toward higher relaxation times) were also observed after the addition of WGA lectin to a solution of **6a**, highlighting the interactions of the spherical micelles with the protein. These modifications can unambiguously be attributed to the specific binding of the nanoparticles with the lectin rather than the sole presence of the protein in the solution as shown by the totally different distribution profile of the WGA lectin alone even at higher concentration (Supporting Information). This result

dx.doi.org/10.1021/la204388h | *Langmuir* 2012, 28, 1418−1426

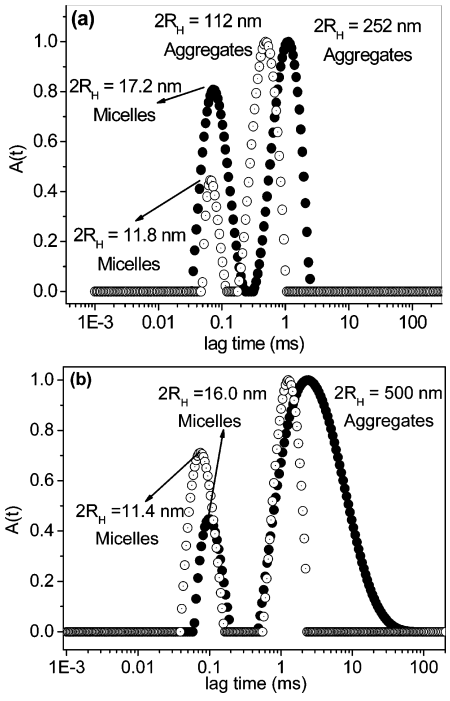

Figure 7. Respective distributions of the relaxation times $A(t)$ from the DLS autocorrelation functions for (a) 0.5 mg/mL **7** in 10 mM PBS buffer, pH 7.2, containing 150 mM NaCl, 0.1 mM $CaCl_2$, and 0.1 mM $MnCl_2$ at 25 °C in the absence (○) and presence (●) of PNA lectin (4 μL, 1.0 mg/mL) and for (b) 1.0 mg/mL **6a** in 10 mM phosphate-buffered saline (pH 7.2) and 150 mM NaCl, 0.1 mM $CaCl_2$, and 0.1 mM $MnCl_2$ at 25 °C in the absence (○) and presence (●) of WGA lectin (2 μL, 1.0 mg/mL).

attests to the presence of the GlcNAc residues on the surfaces of the self-assemblies and their ability to interact specifically with the specific carbohydrate lectin. These experiments clearly demonstrate that PNA and WGA lectins specifically interact with *N*-acetyl-glucosamine and lactose particles, respectively, thus supporting the assumption that the carbohydrates are clearly available on the surfaces of the micelles and can provide specifically labeled nanoparticle systems.

CONCLUSIONS

New glycosylated rod−coil amphiphilic systems have been prepared by the click coupling of sugar residues onto azido-terminated PEG-tetra(*p*-phenylene) precursors. This azide−alkyne synthesis approach offers a very efficient and versatile methodology for introducing any type of carbohydrate structure without requiring numerous protecting-group manipulations and tedious glycosylation reactions. The resulting block copolymer systems have been shown to self-assemble in water into well-defined nanoparticles whose sizes and morphologies were mostly dictated by the amphiphilic balance. As recently reported on PEG_{900}−stearate conjugates,[49] the presence of both a triazolyl ring and a saccharidic ligand does not significantly influence the self-assembly process in terms of size and shape. One can thus expect the formation of objects having specific sizes and geometries mainly by tuning the hydrophilic/hydrophobic balance. In the present study, vesicles were obtained with a PEG_{600} corona whereas highly regular spherical micelles with a mean diameter of 10 nm were observed for the PEG_{900} glycoconjugates as indicated by DLS, TEM, and SAXS characterization. The results are consistent with previous findings from our group[49] and from Kim and colleagues[22,23] on comparable systems. The ability of the self-assemblies to interact with specific carbohydrate lectins was also demonstrated by DLS, confirming the potential of such micelles in medical applications such as diagnosis, drug-delivery systems, and biosensors.

ASSOCIATED CONTENT

Supporting Information

Synthesis and characterization data for compounds **1**−**7** and additional light-scattering data. This material is available free of charge via the Internet at http://pubs.acs.org.

AUTHOR INFORMATION

Corresponding Author

*E-mail: sebastien.fort@cermav.cnrs.fr. Tel: +33 (0)476 03 76 64. Fax: +33 (0)476 54 72 03.

ACKNOWLEDGMENTS

We acknowledge the financial support from CNRS and CAPES-COFECUB (project 620/08). The ESRF and LNLS are acknowledged for supplying the beam time (proposals 02 01 784 and 9967). The technical assistance of Cyrille Rochas during the experiments at ESRF is greatly acknowledged. F.C.G. acknowledges FAPESP (grant 2010/06348-0). Stéphanie Boullanger is acknowledged for the mass spectrometry analyses.

REFERENCES

(1) Sinha, R. *Mol. Cancer Ther.* **2006**, *5*, 1909−1917.
(2) Hillaireau, H.; Couvreur, P. *Cell. Mol. Life Sci.* **2009**, *66*, 2873−2896.
(3) Yuan, F.; Leunig, M.; Huang, S. K.; Berk, D. A.; Papahadjopoulos, D.; Jain, R. K. *Cancer Res.* **1994**, *54*, 3352−3356.
(4) Allen, T. M.; Hansen, C.; Martin, F.; Redemann, C.; Yau-Young, A. *Biochim. Biophys. Acta, Biomembr.* **1991**, *1066*, 29−36.
(5) Basu, S.; Harfouche, R.; Soni, S.; Chimote, G.; Mashelkar, R. A.; Sengupta, S. *Proc. Natl. Acad. Sci. U.S.A.* **2009**, *106*, 7957−7961.
(6) Niikura, K.; Nagakawa, K.; Ohtake, N.; Suzuki, T.; Matsuo, Y.; Sawa, H.; Ijiro, K. *Bioconjugate Chem.* **2009**, *20*, 1848−1852.
(7) Varki, A. *Glycobiology* **1993**, *3*, 97−130.
(8) Raz, A.; Meromsky, L.; Lotan, R. *Cancer Res.* **1986**, *46*, 3667−3672.
(9) Gorelik, E.; Galili, U.; Raz, A. *Cancer Metastasis Rev.* **2001**, *20*, 245−277.
(10) Smart, J. *Adv. Drug Delivery Rev.* **2004**, *56*, 481−489.
(11) Abu-Dahab, R. *Eur. J. Pharm. Sci.* **2001**, *14*, 37−46.
(12) Zhu, J. M.; Yan, F.; Guo, Z. W.; Marchant, R. E. *J. Colloid Interface Sci.* **2005**, *289*, 542−550.
(13) Yamazaki, N. *Adv. Drug Delivery Rev.* **2000**, *43*, 225−244.
(14) Lim, Y. B.; Moon, K. S.; Lee, M. *J. Mater. Chem.* **2008**, *18*, 2909−2918.
(15) Riess, G. *Prog. Polym. Sci.* **2003**, *28*, 1107−1170.
(16) Discher, D. E.; Eisenberg, A. *Science* **2002**, *297*, 967−973.
(17) Giacomelli, C.; Schmidt, V.; Aissou, K.; Borsali, R. *Langmuir* **2010**, *26*, 15734−15744.
(18) Bates, F. S. *Science* **1991**, *251*, 898−905.
(19) Lemarchand, C.; Gref, R.; Lesieur, S.; Hommel, H.; Vacher, B.; Besheer, A.; Maeder, K.; Couvreur, P. *J. Controlled Release* **2005**, *108*, 97−111.
(20) Yamamoto, H.; Kuno, Y.; Sugimoto, S.; Takeuchi, H.; Kawashima, Y. *J. Controlled Release* **2005**, *102*, 373−381.
(21) Sharon, N.; Lis, H. *Glycobiology* **2004**, *14*, 53R−62R.
(22) Kim, B. S.; Hong, D. J.; Bae, J.; Lee, M. *J. Am. Chem. Soc.* **2005**, *127*, 16333−16337.

(23) Kim, B. S.; Yang, W. Y.; Ryu, J. H.; Yoo, Y. S.; Lee, M. *Chem. Commun.* **2005**, 2035−2037.
(24) Kataoka, K.; Harada, A.; Nagasaki, Y. *Adv. Drug Delivery Rev.* **2001**, *47*, 113−131.
(25) Kwon, G. S.; Kataoka, K. *Adv. Drug Delivery Rev.* **1995**, *16*, 295−309.
(26) Rosler, A.; Vandermeulen, G. W. M.; Klok, H. A. *Adv. Drug Delivery Rev.* **2001**, *53*, 95−108.
(27) Chang, D. W.; Dai, L. *J. Mater. Chem.* **2007**, *17*, 364−364.
(28) Ivory, D. M.; Miller, G. G.; Sowa, J. M.; Shacklette, L. W.; Chance, R. R.; Baughman, R. H. *J. Chem. Phys.* **1979**, *71*, 1506−1506.
(29) Hargadon, M. T.; Davey, E. A.; McIntyre, T. B.; Gnanamgari, D.; Wynne, C. M.; Swift, R. C.; Zimbalist, J. R.; Fredericks, B. L.; Nicastro, A. J.; Goodson, F. E. *Macromolecules* **2008**, *41*, 741−750.
(30) Sidorov, V.; Dzekunov, S. M.; Abdallah, D.; Ghebremariam, B.; Roepe, P. D.; Matile, S. *Chem. Commun.* **1999**, 1429−1430.
(31) Hong, D. J.; Lee, E.; Lee, J. K.; Zin, W. C.; Han, M.; Sim, E.; Lee, M. *J. Am. Chem. Soc.* **2008**, *130*, 14448−14449.
(32) Garcia, F.; Fernandez, G.; Sanchez, L. *Chem.—Eur. J.* **2009**, *15*, 6740−6747.
(33) Bae, J.; Choi, J. H.; Yoo, Y. S.; Oh, N. K.; Kim, B. S.; Lee, M. *J. Am. Chem. Soc.* **2005**, *127*, 9668−9669.
(34) Li, Y.; Li, G.; Wang, X.; Li, W.; Su, Z.; Zhang, Y.; Ju, Y. *Chem.—Eur. J.* **2009**, *15*, 6399−6407.
(35) Kolb, H. C.; Finn, M. G.; Sharpless, K. B. *Angew. Chem., Int. Ed.* **2001**, *40*, 2004−2021.
(36) Tornøe, C. W.; Christensen, C.; Meldal, M. *J. Org. Chem.* **2002**, *67*, 3057−3064.
(37) Ma, D. L.; Shum, T. Y. T.; Zhang, F. Y.; Che, C. M.; Yang, M. S. *Chem. Commun.* **2005**, 4675−4677.
(38) Mereyala, H. B.; Gurrala, S. R. *Carbohydr. Res.* **1998**, *307*, 351−354.
(39) Berne, B.; Pecora, R. *Dynamic Light Scattering: With Applications to Chemistry, Biology, and Physics*; Dover Publications: Mineola, NY, 2000.
(40) Provencher, S. W. *Makromol. Chem.* **1979**, *180*, 201−209.
(41) Tammer, M.; Horsburgh, L.; Monkman, A. P.; Brown, W.; Burrows, H. D. *Adv. Funct. Mater.* **2002**, *12*, 447−454.
(42) Giacomelli, C.; Schmidt, V.; Borsali, R. *Macromolecules* **2007**, *40*, 2148−2157.
(43) Pedersen, J. S.; Gerstenberg, M. C. *Macromolecules* **1996**, *29*, 1363−1365.
(44) Choi, J. M.; Kim, Y.; Lee, M. *Appl. Therm. Eng.* **2010**, *30*, 174−180.
(45) Bouzide, A.; LeBerre, N.; Sauve, G. *Tetrahedron Lett.* **2001**, *42*, 8781−8783.
(46) In the distribution of relaxation times $A(t)$ in Figure 2a, the surface area under the peak corresponding to the small-scale structures represents 39% of the total surface area. Thus, assuming that hard-sphere-like particles are present and that the small-scale ($2R_H$ = 10.3 nm) and large-scale ($2R_H$ = 95.0 nm) structures have the same density, the ratio of the number of small-scale structures/number of large-scale structures is given by $N_{small}/N_{large} = (95/10.3)^3(0.390/(1-0.390)) \approx 502$.
(47) Zhang, L. F.; Eisenberg, A. *Macromolecules* **1996**, *29*, 8805−8815.
(48) Burchard, W. *Cellulose* **2003**, *10*, 213−225.
(49) Dal Bó, A. G.; Soldi, V.; Giacomelli, F. C.; Jean, B.; Pignot-Paintrand, I.; Borsali, R.; Fort, S. *Soft Matter* **2011**, *7*, 3453−3461.
(50) Higgins, J. S.; Benoit, H. C. *Polymers and Neutron Scattering*; Clarendon Press: Oxford, U.K., 1994.
(51) Burchard, W. In *Light Scattering from Polymers*; Springer: Berlin, 1983; Vol. *48*, pp 1−124.
(52) Lis, H.; Sharon, N. *Chem. Rev.* **1998**, *98*, 637−674.
(53) Chwalek, M.; Auzely, R.; Fort, S. *Org. Biomol. Chem.* **2009**, *7*, 1680−1688.